Effects of pH on Kinetic Parameters of the Na-HCO_3 Cotransporter in Renal Proximal Tubule

Eitan Gross*#§ and Ulrich Hopfer#

Departments of *Urology and #Physiology and Biophysics, Case Western Reserve University, and §VA Medical Center, Cleveland, Ohio 44106 USA

ABSTRACT The effects of pH on cotransporter kinetics were studied in renal proximal tubule cells. Cells were grown to confluence on permeable support, mounted in an Ussing-type chamber, and permeabilized apically to small monovalent ions with amphotericin B. The steady-state, dinitrostilbene-disulfonate-sensitive current (ΔI) was Na^+ and HCO_3^- dependent and therefore was taken as flux through the cotransporter. When the pH of the perfusing solution was changed between 6.0 and 8.0, the conductance attributable to the cotransporter showed a maximum between pH 7.25 and pH 7.50. A similar profile was observed in the presence of a pH gradient when the pH of the apical solutions was varied between 7.0 and 8.0 (basal pH lower by 1), but not when the pH of the basal solution was varied between 7.0 and 8.0 (apical pH lower by 1 unit). To delineate the kinetic basis for these observations, ΔI-voltage curves were obtained as a function of Na^+ and HCO_3^- concentrations and analyzed on the basis of a kinetic cotransporter model. Increases in pH from 7.0 to 8.0 decreased the binding constants for the intracellular and extracellular substrates by a factor of 2. Furthermore, the electrical parameters that describe the interaction strength between the electric field and substrate binding or charge on the unloaded transporter increased by four- to fivefold. These data can be explained by a channel-like structure of the cotransporter, whose configuration is modified by intracellular pH such that, with increasing pH, binding of substrate to the carrier is sterically hindered but electrically facilitated.

INTRODUCTION

More than 80% of the filtered load of HCO_3^- in the mammalian kidney is reabsorbed in the proximal tubule, with the remaining 20% reabsorbed by the more distal tubule segments. Thus the proximal tubule plays a major role in maintaining acid-base balance. The proximal tubule epithelium achieves this task by secreting protons into the lumen and an equal number of base equivalents across the basolateral plasma membrane into the peritubular medium. The primary transporters involved in proximal tubular reabsorption of HCO_3^- are shown in Fig. 1. The principal pathway for uphill movement of acid from cell to tubular fluid is via the luminal membrane Na^+/H^+ exchanger (Aronson, 1983). The major transport pathway for HCO_3^- exit across the basolateral membrane is the Na-HCO_3 cotransporter (Boron and Boulpaep, 1983a; Alpern, 1985; Alpern and Chambers, 1986; Biagi and Sohtell, 1986). To maintain intracellular Na^+ and pH homeostasis, under conditions of high through flux, Na^+ and HCO_3^- reabsorption in these cells must be regulated in a coordinated manner. Na^+/H^+ exchange activity was found to be regulated by an internal H^+ modifier site in various tissues (Aronson et al., 1982; Boron and Boulpaep, 1983b; Grinstein et al., 1984). Soleimani et al. (1991) have suggested that H^+ inhibits the binding of Na^+ to the Na-HCO_3 cotransporter, through binding to an allosteric site on the protein. Studying the effect of changing the intra- and extracellular pH on the Na^+-Na^+ exchange rate of the Na-HCO_3 cotransporter in basolateral membrane vesicles, they found it to be sensitive to changes in intracellular but not to extracellular pH. They suggested an H^+ allosteric binding site to explain their data, which is located on the cytoplasmic side of the cotransporter protein. Although that study provided important information on the effect of pH on the Na^+-Na^+ exchange rate, this partial transport mode may not be relevant to net transport of $NaHCO_3$, which is the physiologically important aspect of the transport process. To address this issue we studied the effects of pH on the net flux of $NaHCO_3$ through the cotransporter, as measured by electrical current across apically permeabilized monolayers of proximal tubular cells. The data were analyzed based on a kinetic model that we recently published (Gross and Hopfer, 1998).

A number of transporters have been cloned and expressed in oocytes of the amphibian *Xenopus* (Parent et al., 1992; Hager et al., 1995; Panayotova-Heiermann et al., 1995; Boorer et al., 1996; Klamo et al., 1996; Mackenzie et al., 1996, 1998; Eskandari et al., 1997; Forster et al., 1998). While enabling researchers to characterize the different transport modes and develop detailed mathematical models of many transporters, the *Xenopus* oocyte is an exogenous expression system that lacks the native intracellular environment and potential regulatory accessory proteins that may be important determinants of the kinetic properties of these transporters in their native state. Indeed, initial analyses of the HCO_3^-:Na^+ stoichiometry of rat kidney clone of the Na-HCO_3 cotransporter (rkNBC) expressed in *Xenopus* oocytes, based on reversal potential, indicated a ratio of 2:1 (Muller-Berger et al., 1998). This stoichiometry is different

Received for publication 15 July 1998 and in final form 29 March 1999.

Address reprint requests to Dr. Eitan Gross, Research Department, VA Medical Center, 10701 East Blvd, MS151(W), Cleveland, OH 44106. Tel.: 216-791-3800, ext. 3244; Fax: 216-229-8509; E-mail: ezg@po.cwru.edu.

© 1999 by the Biophysical Society

0006-3495/99/06/3066/10 $2.00

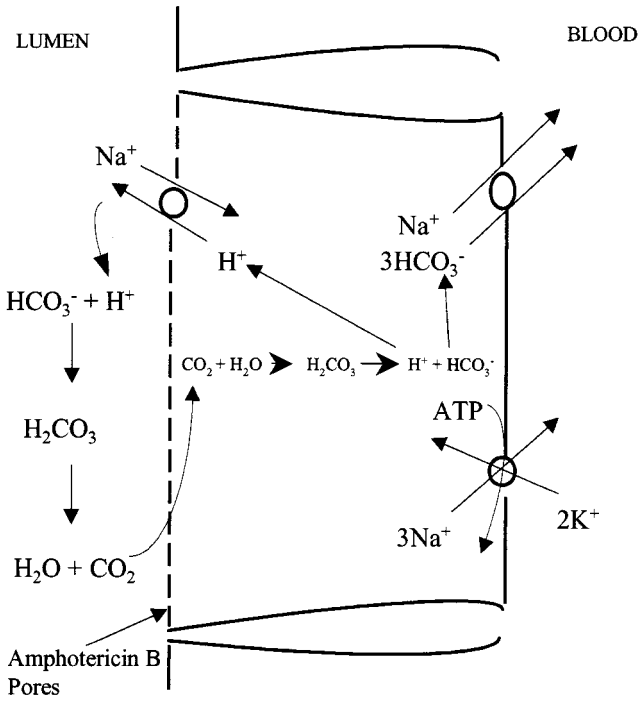

FIGURE 1 Schematic presentation of the cellular transport model on which experiments were based. The Na-HCO_3 cotransporter transports two net negative charges. Apical application of amphotericin B functionally "removes" the apical membrane for electrical measurements.

from the 3:1 ratio measured in intact proximal tubule cells (Yoshitomi and Frömter, 1985; Gross and Hopfer, 1996). Furthermore, it is insufficient to mediate HCO_3^- efflux in intact proximal tubule cells at the existing membrane potential of approximately −60 mV (Yoshitomi and Frömter, 1985; Coppola and Frömter, 1994; Gross and Hopfer, 1995). To the best of our knowledge, the present study is one of the few to present detailed kinetics of a cotransporter in a native, intact epithelium.

MATERIALS AND METHODS

Cell culture

Experiments were carried out with the rat proximal tubular cell line SKPT-0193 Cl.2 (Woost et al., 1996). The line is derived from microdissected primary cultures of the S1 region of the proximal tubule. Passages 50 to 70 were used for the reported experiments. Cells were grown on collagen-coated (20% bovine hoof collagen in 60% ethanol) Millicell-CM filters (area = 0.6 cm^2) in a 1:1 mixture of Dulbecco's modified essential medium and Ham's F12, supplemented with 15 mM HEPES, 1.2 mg/ml $NaHCO_3$, 5 μg/ml insulin, 5 μg/ml transferrin, 5 ng/ml epithelial growth factor, 4 μg/ml dexamethasone, and 10% fetal bovine serum. Typically, 3×10^5 cells were seeded and grown to confluence in 5 days. Light microscopy showed a "cobblestone" appearance, which is typical for epithelial cells.

Electrophysiology

Confluent cells have a low basal monolayer conductance of 0.5–1 mS/cm^2, indicating low ion permeability of tight junctions. This low baseline conductance allows the detection of electrical signals from cellular transporters that make only small contributions to the overall monolayer conductance. Filters with cells were mounted horizontally in an Ussing-type chamber (Analytical Bioinstrumentation, Cleveland, OH) equipped with voltage and current electrodes. Only cell monolayers with an initial conductance of 1 mS/cm^2 or less were used in the experiments described here. Electrophysiological measurements were made with a voltage-clamp module (model 558-C-5; Bioengineering, University of Iowa, IA) controlled by an IBM PC via the DATAQ software package (Dataq Instruments, Akron, OH). Current and voltage were recorded with a strip chart recorder and in parallel through an A/D converter on a microcomputer. The apical and basolateral compartments of the Ussing chamber had a volume of 0.5 ml each. The cells were perfused on each side of the monolayer separately with a peristaltic pump at a rate of ~2 ml/min. The chamber and all solutions were maintained in a heated incubator, allowing control of CO_2 pressure (P_{CO2}) and temperature.

All solutions were first adjusted for pH with acetic acid and then preequilibrated with CO_2 at the appropriate P_{CO2} for 1 h. The pH of the solutions was measured and adjusted again before the beginning of the experiment and was measured once more at the end of each experiment. The solutions were maintained at the appropriate P_{CO2} throughout the entire experiment, and the pH was found to change by less than 0.1. Experiments were carried out at 37°C. CO_2 pressure was continuously monitored with a CO_2 monitor (Puritan-Bennett, Los Angeles, CA). For composition of solutions, refer to the appropriate figure legends.

To measure the cotransporter-related current, cell monolayers were permeabilized with 10 μM apical amphotericin B as described previously (Gross and Hopfer, 1996), and the 4,4′-dinitrostilbene-2,2′-disulfonic acid (DNDS)-sensitive current was taken as flux through the cotransporter. Current-voltage (*I-V*) relations were obtained by stepping the voltage between −100 and +100 mV in 20-mV increments. The DNDS-sensitive (ΔI-*V*) curves were obtained by first measuring an *I-V* curve in the absence of DNDS and then after 10 min of basolateral perfusion of DNDS. All reported currents, except for those in Fig. 2, are difference currents (ΔI); ΔI_{sc} refers to the difference current measured under short-circuit conditions, driven by ion gradient(s).

Materials

Amphotericin B, bovine serum albumin, HEPES, D-glucose, *N*-methyl-D-glucamine (NMDG), gluconic acid, and all salts were purchased from Sigma Chemical Co. (St. Louis, MO). Acetic acid was from Fisher Scientific. 4,4′-Dinitrostilbene-2,2′-disulfonic acid (DNDS) was obtained from Pfaltz and Bauer (Waterbury, CT). Bovine hoof collagen was a generous gift from Ethicon (Somerville, NJ).

Computer simulations

All fitting procedures were performed with the SCoPFit simulation package (SCoP Simulations, Berrien Springs, MI), as previously described (Gross and Hopfer, 1998). The program uses the "principal axis" (praxis) algorithm to automatically search for a global minimum in the error function, by changing the initial value of each parameter by a predetermined fraction (the maximum step). A multistage approach was employed, in which the magnitude of the maximum step was progressively decreased to fine-tune the search process. The algorithm also includes occasional random jumps in the maximum step to avoid confinement to a local minimum in the parameter space. Typically, ~3000 iterations were performed during which translocation, and binding/dissociation rate constants were allowed to vary over a wide range, until a minimum in the error function (χ^2) was reached.

Statistics

Experiments were conducted in quadruplicate. The data listed in Table 2 are means ± SE. The probability distribution for the reduced χ^2 (i.e., $P\chi^2_n$;

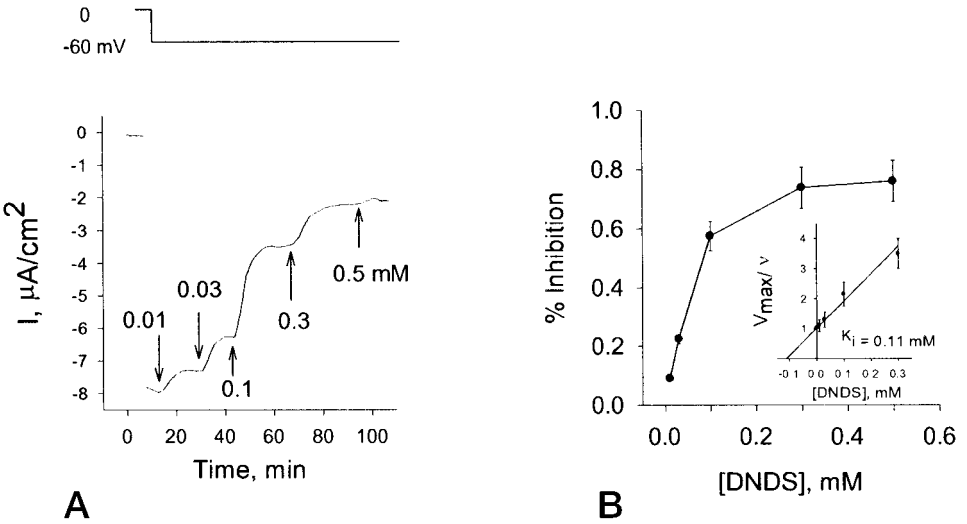

FIGURE 2 Dose-response relationship for the inhibition of cotransporter activity by DNDS. (*A*) Apically permeabilized cells were perfused with symmetrical solutions containing 10 mM Na^+ and 18 mM HCO_3^-. To activate the cotransporter, V was clamped to −60 mV. DNDS was then added basolaterally at the indicated times and concentrations. (*B*) Percentage inhibition of the maximum current by DNDS as determined from *A*. Maximum inhibition is obtained at ~0.5 mM DNDS. (*Inset*) Dixon analysis of the data shown in *B* yields a K_i of 0.11 mM DNDS.

Bevington, 1969) was used to assess the goodness of fit of model equations to experimental data, where n is the degree of freedom (i.e., number of data points − number of fitted parameters). To estimate the approximate information content of *I-V* curves, they were fitted by arbitrary polynomial equations, and the best fit was determined by the minimum χ^2 (Bevington, 1969). The number of parameters of the best-fitted polynomial was assumed to give a maximum for the number of parameters that could unequivocally be determined for any kinetic model.

RESULTS

Experimental strategy

Fig. 1 illustrates the primary transporters involved in Na^+ and HCO_3^- reabsorption in the proximal tubule (Emmett et al., 1992). The transporters associated with electrical charge movement are located in the basolateral plasma membrane. These include the Na,K-ATPase and the Na^+-HCO_3^- cotransporter. To reveal cotransporter activity to external electrodes, 10 μM amphotericin B was added to the apical solution of proximal tubule monolayers in an Ussing chamber. Amphotericin B is a polyene ionophore that renders the plasma membrane permeable to small monovalent ions (Na^+, K^+, Cl^-), but not to those with higher valences, such as Ca^{2+} (Kirk and Dawson, 1983). The increased permeabilization stays restricted for several hours to the plasma membrane to which it was added. The property is a result of a requirement for cholesterol and the relatively high cholesterol content of the plasma membrane compared to intracellular membranes (Kirk and Dawson, 1983). This protocol also allows to vary cytosolic Na^+ and HCO_3^- concentrations in a controlled manner, because small ions equilibrate between apical solution and cytosol. The use of amphotericin B for these purposes is a common practice in studies of epithelial transport (Kirk and Dawson, 1983; Backman et al., 1992; Illek et al., 1993; Acevedo, 1994; Gross and Hopfer, 1996, 1998). In a previous study, we found that Na,K-ATPase and a spontaneously increasing Cl^- conductance in the basolateral plasma membrane interfered with the accurate determination of current through the cotransporter. Therefore, contributions of these two transporters to the electrical current were eliminated by solutions that were K^+-free (replaced by *N*-methyl-D-glucamine) and Cl^--free (replaced by gluconate).

Dose-response for dinitrostilbenedisulfonate

The Na^+-bicarbonate cotransporter is inhibited by stilbenedisulfonates (Boron and Knakal, 1989). DNDS does not interact covalently with proteins and is therefore a convenient, reversible inhibitor for defining the DNDS-sensitive current or conductance of the basolateral plasma membrane. We had previously shown that this DNDS-sensitive current is identical to the Na^+- and HCO_3^--dependent current in proximal tubule SKPT cells, provided K^+- and Cl^--free media are used, so that it can be taken as current through the cotransporter. To better define the potency of DNDS, as an inhibitor, a dose-response curve was established. Apically permeabilized proximal tubule monolayers were perfused on both sides with the same solution containing 10 mM Na^+ and 18 mM HCO_3^-, with current generated by applying a voltage of −60 mV across the monolayer. As shown in Fig. 2, ~75% of the current can be inhibited by 0.5 mM DNDS, indicating that we had selected conditions in which a large portion of the total conductance could be attributed to the Na^+-bicarbonate cotransporter. A detailed analysis of the dose-response curve indicated a K_i for DNDS of 0.11 mM and maximum inhibition by 0.5 mM. A supramaximum concentration of 1 mM DNDS was used in subsequent experiments to define the DNDS-sensitive current.

Effects of pH on cotransporter current

To evaluate whether the cotransporter was affected by pH, its activity was measured as a function of pH with identical solutions on both sides. The pH was varied between 6.00 and 8.00, and cotransporter activity measured as DNDS-sensitive current. The HCO_3^- concentration was kept con-

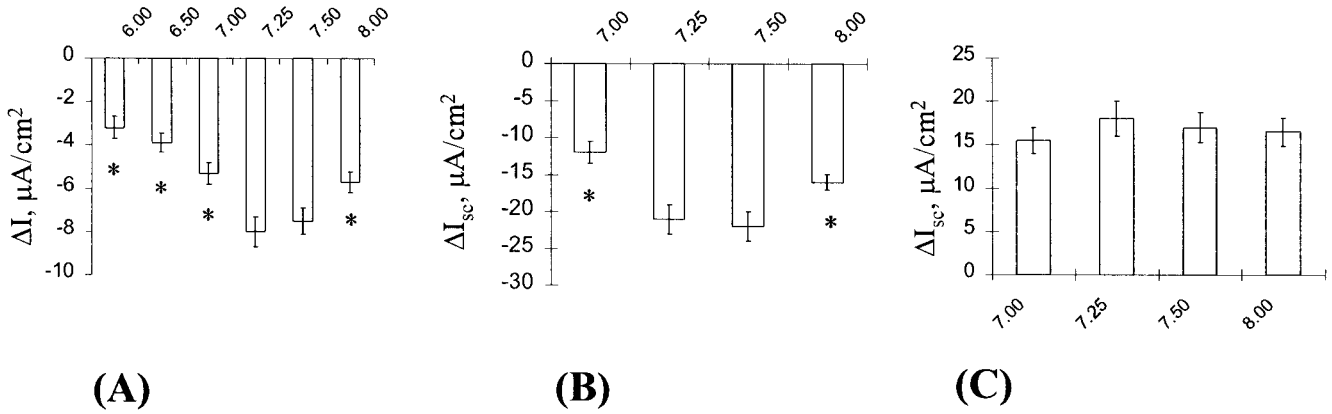

FIGURE 3 Effect of pH on DNDS-sensitive current under three different conditions. (*A*) pH of the apical and basolateral solutions was changed in a symmetrical manner between pH 6.00 and pH 8.00. Currents were measured at −60 mV. (*B*) A pH gradient of 1.0 (high on the apical side, low on the basolateral side) was applied across the monolayer. The pH of the apical solution was varied between 7.00 and 8.00. Currents were measured at 0 mV (I_{sc}). (*C*) A pH gradient of 1.0 (high on the basolateral side, low on the apical side) was applied across the monolayer. The pH of the basolateral solution was varied between 7.00 and 8.00. Currents were measured at 0 mV (I_{sc}). Basolateral and apical solutions contained (in mM) 10 Na gluconate, 2.5 Ca gluconate, 1.1 Mg gluconate, 100 HEPES, 25 D-glucose, 50 NMDG, 18 HCO_3^-, and 0.1% BSA. Bicarbonate concentration of apical and basolateral solutions in *A* was 18 mM. In *B*, bicarbonate concentration of apical solutions was 18 mM, and that of basolateral solution was 1.8 mM. In condition *C*, bicarbonate concentration of basolateral solutions was 18 mM, and that of apical solution was 1.8 mM. $*P < 0.05$, compared with ΔI at pH 7.5.

stant, while the pH changed, by adjusting the CO_2 concentration as calculated from the Henderson-Hasselbalch equation. Fig. 3 *A* shows an analysis of current measured at −60 mV from this series of experiments. The Δ*I*-pH profile exhibits a maximum between 7.25 and 7.50. These results suggest the presence of a pH-regulated site on one or both sides of the basolateral plasma membrane.

To localize the pH effect, the apically permeabilized cell monolayers were again perfused with solutions of varying pH between 7.00 and 8.00. However, in contrast to the initial evaluation, a pH gradient of 1 unit was established so that only one side was exposed to the pH range between 7.00 and 8.00 and the pH on the other varied between 6.00 and 7.00. These experiments were based on the assumptions that 1) CO_2 rapidly equilibrates across the basolateral plasma membrane, and 2) CO_2, H^+, and HCO_3^- are in equilibrium according to the Henderson-Hasselbalch relation. In other words, CO_2 movement across the membrane and CO_2 hydration/dehydration were assumed to be rapid compared to H^+ and HCO_3^- fluxes across the basolateral plasma membrane. Consequently, a 10-fold H^+ gradient (difference of 1 pH unit) is associated with a 10-fold HCO_3^- gradient in the opposite direction.

To test the validity of the above assumptions, the reversal potential of the cotransporter was measured for a 10-fold HCO_3^- gradient. This reversal potential is given at 37°C by the thermodynamic equivalent of the Nernst potential (Gross and Hopfer, 1996), $E_{rev} = 60/(m - 1)\log\{([Na^+]_i [HCO_3^-]_i^3)/([Na^+]_o[HCO_3^-]_o^3)\}$, where m is the number of HCO_3^- anions cotransported with each Na^+ cation. Fig. 4 shows the DNDS-sensitive current as a function of voltage (Δ*I*-*V*) in the presence of a 10-fold HCO_3^- gradient, measured at several different pH values. The observed reversal potential under these conditions was ~80 mV, which corresponds to $m = 3.2$. The measured reversal potential is close to the expected value of 90 mV when $m = 3.0$. The close agreement between expected and measured reversal potential supports the assumption that pH and bicarbonate gradients can be established and maintained across the basolateral plasma membrane of epithelial monolayers that have been permeabilized with amphotericin B on the apical side.

The pH dependence of the DNDS-sensitive current at 0 mV (ΔI_{sc}) in the presence of a pH gradient is shown in Fig. 3, *B* and *C*. A comparison of the data in Fig. 3, *B* and *C*, with those in Fig. 3 *A* indicates that the apical/cytosolic pH, but not the basolateral pH, between 7.00 and 8.00, modulates the kinetics of the Na-HCO_3 cotransporter.

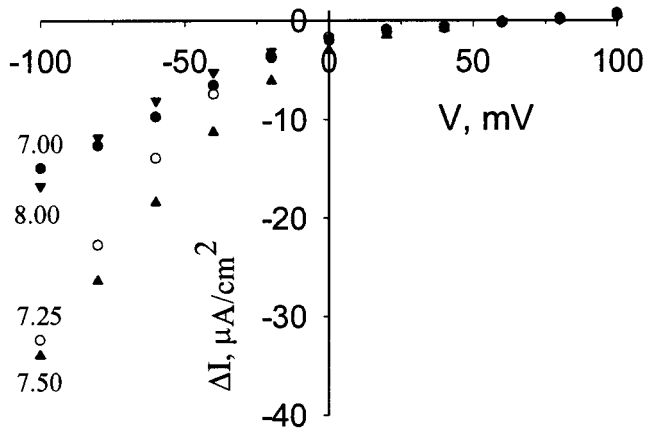

FIGURE 4 DNDS-sensitive current-voltage (Δ*I*-*V*) relationships of the cotransporter under a 10-fold bicarbonate concentration gradient (higher on the apical side). Solution compositions are as described in the legend to Fig. 3 *B*.

Cotransporter kinetics

The biphasic shape of the current-pH profile in Fig. 3, *A* and *B*, suggests the presence of titratable sites on the cotransporter that affect its conformation and kinetics. To evaluate whether pH affected specific kinetic steps in the catalytic cycle of the cotransporter, cotransporter current-voltage (ΔI-V) curves were analyzed on the basis of a detailed kinetic transport model that was described recently (Gross and Hopfer, 1998). This model specifically takes into account the effects of membrane potential and of Na^+ and HCO_3^- concentrations on both sides of the membrane. It consists of one transport loop linking six discrete states of the carrier without assumptions about rate limiting or potential-sensitive steps (Fig. 5). Interestingly, an analytical expression could be derived from the model that describes the steady-state current generated by the coupled flux of Na^+ and HCO_3^- through the cotransporter (Eq. 13) and can consequently be used for fitting experimental data.

The model specifically takes into account the effects of the membrane potential on ion binding and dissociation reaction steps as well as on the translocation rates. Based on Eyring's theory of reaction rates (Eyring et al., 1949; Woodbury, 1971), the binding of Na^+ and HCO_3^- is described as a series of activated processes in which Na^+ and HCO_3^- hop across a series of symmetrical Eyring barriers. The energy barrier for each step is modulated by the fraction of the electrical field across the membrane that is sensed by this step.

The modulation factor is given by $e^{-\zeta x u/2}$, where ζ is the valence of the carrier species corresponding to that step; x is the corresponding fraction of the membrane potential sensed by that step; and u is the reduced, dimensionless membrane potential, $u = FV/RT$, where V is the membrane potential and F, R, and T have their usual meanings. A detailed account of the model is given in Gross and Hopfer (1998). The general forms of the apparent rate constants for the model are given below:

$$f_1 = f_1^o[Na^+]_i^n \exp(n\alpha' u/2);$$

Binding of intracellular Na^+ to the carrier (1)

$$b_1 = b_1^o \exp(-n\alpha' u/2);$$

Dissociation of intracellular Na^+ from the carrier (2)

$$f_2 = f_2^o[HCO_3^-]_i^m \exp(-m\beta' u/2);$$

Binding of intracellular HCO_3^- to the carrier (3)

$$b_2 = b_2^o \exp(m\beta' u/2);$$

Dissociation of intracellular HCO_3^- from the carrier (4)

$$f_3 = f_3^o \exp((z\delta_z + n\delta_n - m\delta_m)u/2);$$

Translocation of the loaded carrier (inside→outside) (5)

$$b_3 = b_3^o \exp(-(z\delta_z + n\delta_n - m\delta_m)u/2);$$

Translocation of the loaded carrier (outside→inside) (6)

$$f_4 = f_4^o \exp(-m\beta'' u/2);$$

Dissociation of extracellular HCO_3^- from the carrier (7)

$$b_4 = b_4^o[HCO_3^-]_o^m \exp(m\beta'' u/2);$$

Binding of extracellular HCO_3^- to the carrier (8)

$$f_5 = f_5^o \exp(n\alpha'' u/2);$$

Dissociation of extracellular Na^+ from the carrier (9)

$$b_5 = b_5^o[Na^+]_o^n \exp(-n\alpha'' u/2);$$

Binding of extracellular Na^+ to the carrier (10)

$$f_6 = f_6^o \exp(-z\delta_z u/2);$$

Translocation of the unloaded carrier (outside→inside) (11)

$$b_6 = b_6^o \exp(z\delta_z u/2);$$

Translocation of the unloaded carrier (inside→outside) (12)

where z is the valence of the empty carrier, n and m are the number of Na^+ and HCO_3^- ions being transported, and δ_n and δ_m represent the fractions of the electric field through which Na^+ and HCO_3^- ions, respectively, move with transport across the membrane. δ_z is the corresponding parameter that describes the fraction of the electric field sensed by the charge on the unloaded carrier as it traverses the membrane. α' and α'' represent the fraction of the electric field sensed by the binding steps of cytoplasmic and extracellular, basolateral Na^+, respectively, and $\alpha' + \alpha'' + \delta_n = 1$ (see also Läuger and Jauch, 1986). β' and β'' represent the corre-

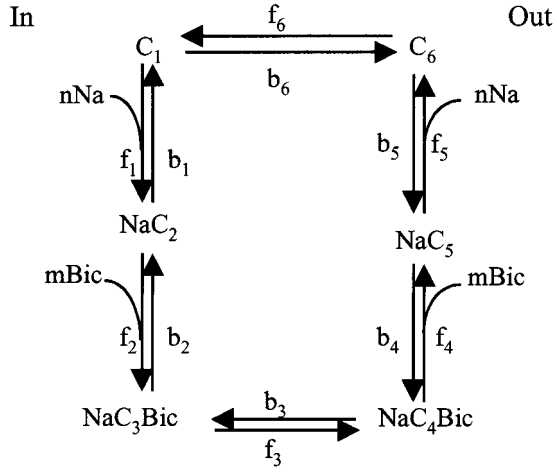

FIGURE 5 A six-state ordered-binding transport model of the Na-HCO_3 cotransporter. The binding of three HCO_3^- anions to the carrier is described as a single, lumped step (see Gross and Hopfer, 1998, for details).

sponding parameters for bicarbonate, with $\beta' + \beta'' + \delta_m = 1$. It should be noted that no constraint or limit can be written to describe the translocation of the charge z associated with the empty carrier. The reason for this lack of constraint is that unlike the Na^+ and HCO_3^- ions, the charge z does not necessarily traverse the entire distance of membrane thickness upon translocation of the substrates across the membrane. The product $z\delta_z$ can thus assume any value. Furthermore, z and δ_z cannot be determined separately. The product $z\delta_z$ will thus be referred to as the "effective charge" of the unloaded carrier.

The net current, generated by the flux of Na^+ and HCO_3^- through the cotransporter, can now be expressed as the sum of all possible translocation steps:

$$I = -F\{z\delta_z(b_6C_1 - f_6C_6) + (z\delta_z + n - m)(f_3C_3 - b_3C_4)\} \quad (13)$$

where C_x is the membrane density of the corresponding carrier state. Only the empty (C_1, C_6) and fully loaded (C_3, C_4) forms of the carrier were assumed to be able to translocate across the membrane. This assumption is consistent with the observations that no CO_2-dependent DNDS-sensitive current could be observed in the absence of Na^+ (see also Fig. 2 in Gross and Hopfer, 1998), and that no Na^+-dependent DNDS-sensitive current could be observed in the absence of CO_2. Equation 13 can be solved for any C_x in terms of the 12 rate constants.

In a previous study, the HCO_3^- to Na^+ stoichiometry was determined as 3:1, based on the measured reversal potential and thermodynamic considerations. These values were used for the present kinetic analysis.

The numerical values of the rate constants and electrical coefficients were determined for four pH values by fitting measured ΔI-V curves with Eq. 13. For each pH value, at least seven ΔI-V curves with different Na^+ and HCO_3^- concentrations were fitted to a single set of parameters. The numerical results of the fits are shown in Table 1. Representative examples of primary ΔI-V data and theoretical curves based on the fits from Table 1 are shown in Fig. 6 for different Na^+ concentrations and Fig. 7 for different HCO_3^- concentrations.

Whereas the absolute values of the rate constants in Table 1 have no physical meaning because of an arbitrary assumption about the membrane density of the cotransporter, the ratio of rate constants provides valid kinetic information about cotransporter function, within the usual limits of kinetic models. Similarly, the electrical interaction coefficients can be given physical meaning. Table 2 summarizes significant effects of pH on the ratios of binding to dissociation constants (r^o) for intracellular and extracellular Na^+ and HCO_3^-, as well as on the electrical modulation of HCO_3^- and Na^+ binding β and α, respectively.

Interestingly, the binding constants (r^o) of Na^+ and bicarbonate on both sides of the basolateral membrane de-

TABLE 1 Numerical values of fitted parameters obtained by fitting the *I–V* relations at each pH by Eq. 13

Parameter	pH 7.00	pH 7.25	pH 7.50	pH 8.00	Sensitivity
$z\delta_z$	0.4	1.3	1.4	1.5	−0.2
α'	0.03	0.04	0.08	0.15	−0.026
α''	0.03	0.04	0.08	0.15	+0.024
β'	0.06	0.1	0.2	0.25	+0.03
β'''	0.06	0.1	0.2	0.25	−0.04
f_1^o (M^{-1} s^{-1})	64	65	57	47	+0.58
b_1^o (s^{-1})	1.0	1.4	1.6	1.7	−0.16
f_2^o (M^{-3} s^{-1})	$2.0 \cdot 10^7$	$1.9 \cdot 10^7$	$1.5 \cdot 10^7$	$1.3 \cdot 10^7$	+0.22
b_2^o (s^{-1})	$4.0 \cdot 10^4$	$4.5 \cdot 10^4$	$5.0 \cdot 10^4$	$5.0 \cdot 10^4$	−0.21
f_3^o (s^{-1})	$7.0 \cdot 10^3$	$7.0 \cdot 10^3$	$7.3 \cdot 10^3$	$1.0 \cdot 10^4$	+0.21
b_3^o (s^{-1})	$2.5 \cdot 10^3$	$2.5 \cdot 10^3$	$4.2 \cdot 10^3$	$5.0 \cdot 10^3$	−0.18
f_4^o (s^{-1})	$1.5 \cdot 10^3$	$1.7 \cdot 10^3$	$1.9 \cdot 10^3$	$2.0 \cdot 10^3$	+0.19
b_4^o (M^{-3} s^{-1})	$1.4 \cdot 10^6$	$1.3 \cdot 10^6$	$1.2 \cdot 10^6$	$1.0 \cdot 10^6$	−0.16
f_5^o (s^{-1})	1.1	1.3	1.6	1.7	+0.34
b_5^o (M^{-1} s^{-1})	65	61	53	50	−0.09
f_6^o (s^{-1})	0.5	0.5	0.3	0.3	+0.24
b_6^o (s^{-1})	0.8	0.8	0.3	0.3	+0.23
C_T (pmol/cm^2)	0.2	0.2	0.2	0.2	
n	1	1	1	1	
m	3	3	3	3	
$P^2_{\chi n}$	>0.95	>0.95	>0.95	>0.95	

$P^2_{\chi n}$ is the probability distribution for the reduced χ^2.

The information content of each ΔI–V curve is equivalent to four parameters, as each curve could be best fitted by a cubic polynomial, with $P\chi^2_n > 0.99$. A minimum of five ΔI–V curves, under separate conditions of [Na^+], [HCO_3^-], is required to determine the value of all free 16 parameters at any pH value, as the 0,0 intercept of four of the five curves represents duplicate information. However, in practice, seven to eight different ΔI–V curves were used to determine the kinetic parameters at each pH value.

The numerical values for the parameters C_T, n, and m were kept fixed.

Sensitivity was measured at pH 7.50 and at −60 mV by dividing the fractional change in current by a fractional change in parameter. The sensitivity of b_6^o was calculated as the difference between unity and the sum of the sensitivities of all other parameters.

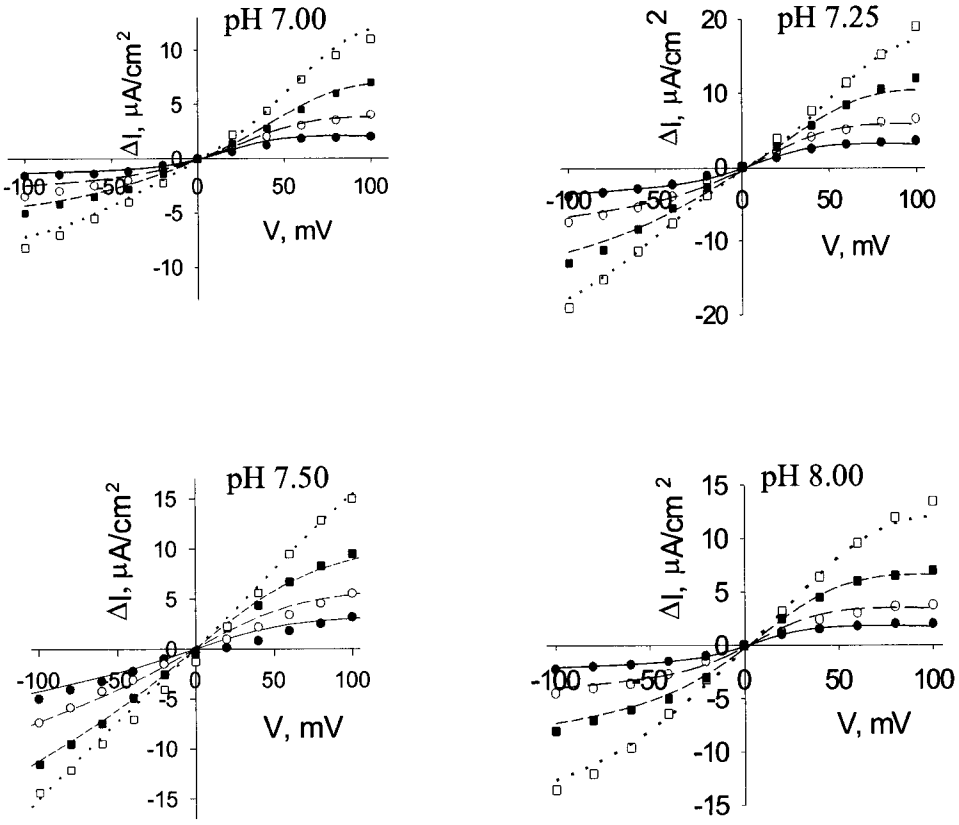

FIGURE 6 Steady-state DNDS-sensitive currents (ΔI) as a function of voltage (V) at 2.5 mM (●), 5.0 mM (○), 10 mM (■), and 20 mM (□) Na^+. The concentration of Na^+ was varied by replacing NMDG with Na gluconate. The concentration of HCO_3^- was 30 mM, and that of the other components was as in Fig. 3. Apical and basolateral solutions were symmetrical. Lines through the data points are model predictions (Eq. 13).

creased by a factor of ~2 when the pH increased from 7.0 to 8.0. Furthermore, all electrical parameters [electrical modules of Na^+ (α) and of HCO_3^- (β) binding and effective charge of the unloaded transporter ($z\delta_z$)] increased by about four- to fivefold (Table 1).

DISCUSSION

The kinetic model contains a relatively large number (i.e., 16) of free parameters. Therefore, it was of interest whether the steady-state current data from monolayers contained enough information to obtain stable fits. That was apparently the case because the fits were internally consistent and described monotonic, nonrandom changes in the binding of ions on both sides and in the electrical interaction coefficients, α, β, and $z\delta_z$ with pH. The ΔI-V curves are nonlinear at both high positive and high negative potentials and therefore contain considerable kinetic information. In addition, the information of all ΔI-V curves at a given pH under different conditions of [Na^+] and [HCO_3^-] were used for a single set of parameters.

The estimated values for rate constants and electrical parameters in the present study (Table 1) differ from those obtained previously (corrected Table 2, *Biophys J.* 76:1720, 1999). Are these differences statistically significant, and how can they be explained? The experimental data in the present study were obtained with identical solutions on both sides of the monolayer, while transport was previously

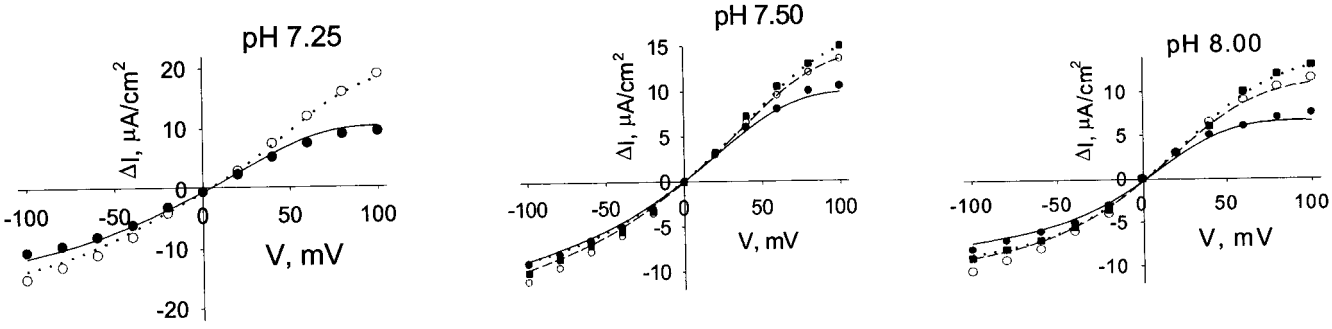

FIGURE 7 Steady-state DNDS-sensitive currents (ΔI) as a function of voltage (V) at 10 mM (●), 30 mM (○), and 57 mM (■) HCO_3^-. The concentration of all other components was as in Fig. 3. Lines through the data points are model predictions (Eq. 13).

TABLE 2 Effect of pH on the ratio of binding/dissociation rate constants (r°) of the intracellular and extracellular substrates, the electrical modulation of Na^+ and HCO_3^- binding (α and β, respectively, at −60 mV), and the ratio of membrane translocation rates of the loaded and unloaded carrier (f_3°/b_3° and f_6°/b_6°, respectively)

	pH 7.00	pH 7.25	pH 7.50	pH 8.00
r°_{Nai}	64 ± 6	46 ± 5	36 ± 4	28 ± 3
r°_{Nao}	59 ± 6	47 ± 8	33 ± 4	29 ± 2
r°_{Bici}	500 ± 52	422 ± 45	300 ± 34	260 ± 18
r°_{Bico}	933 ± 94	765 ± 82	632 ± 62	500 ± 44
β^*	1.5 ± 0.2	2.0 ± 0.3	3.9 ± 0.5	5.4 ± 0.6
$\alpha^\#$	1.1 ± 0.1	1.1 ± 0.1	1.2 ± 0.1	1.4 ± 0.1
f_3°/b_3°	2.8 ± 0.2	2.8 ± 0.3	1.7 ± 0.2	2.0 ± 0.3
f_6°/b_6°	0.6 ± 0.02	0.6 ± 0.05	1.0 ± 0.1	1.0 ± 0.1

$^*\beta_{Bic} = \exp(-m\beta' u/2)/\exp(m\beta' u/2)$.
$^\#\alpha_{Na} = \exp(-n\alpha' u/2)/\exp(n\alpha' u/2)$.

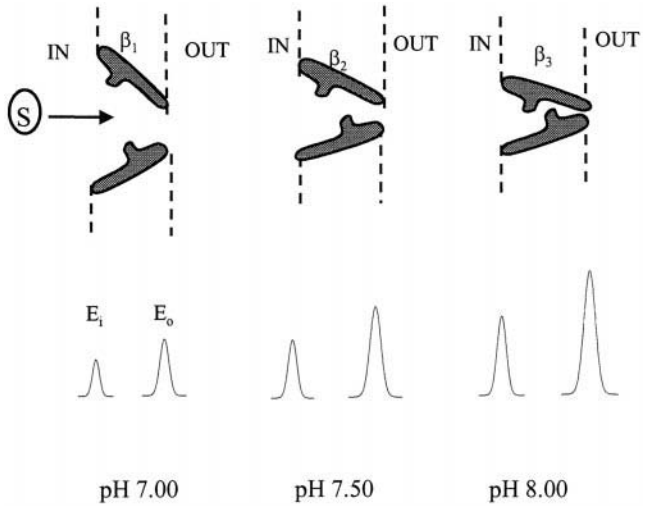

FIGURE 8 Schematic presentation of the proposed "gated channel" model for the Na-HCO_3 cotransporter. The cotransporter alternates between an "inward-facing" and an "outward-facing" conformation (*top*). In the "inward-facing" conformation, the height of the Eyring energy barrier for the binding of intracellular substrate (E_i) is lower than that for the extracellular substrate (E_o) (*bottom*). As a result, the probability for the binding of the intracellular substrates to the cotransporter is larger than that for the extracellular substrates. The composite binding function of the substrates exhibits a maximum at pH 7.50.

measured under zero-*trans* conditions for sodium. By definition, the data obtained under zero-*trans* conditions can provide only very coarse estimates of the rate constants on the *trans* side, because the zero-*trans* conditions make reactions on the *trans* side virtually irreversible. Therefore, fits (χ^2) of the zero-*trans* data were calculated using the parameters estimated in this study as well as those in the previous study, whereby the total transporter concentration was treated as an adjustable parameter. An F-test analysis indicates that, based on statistical criteria, the zero-*trans* data are equally well fitted by both sets of rate constants and electrical parameters; i.e., any difference is not statistically significant ($p < 0.05$).

The results obtained in this study are particularly interesting because a detailed kinetic scheme was used to explain data obtained from the cotransporter in its native plasma membranes and in cells with a native monolayer configuration. They provide a crucial basis for comparison with data from expression systems (Muller-Berger et al., 1998). For several transporters now, discrepancies have been described in their behavior between native and foreign environments. For example, in the case of the Na^+/H^+ exchanger NHE3, the presence or absence of adapter proteins influences the activation by protein kinase A (Yun et al., 1998).

How can the kinetic model contribute to our ideas about the physical behavior of the cotransporter? We propose a carrier model for the Na-HCO_3 cotransporter with "channel-like" properties and a single binding site for each substrate that is accessible from either the intracellular side or the extracellular side (Fig. 8). The result that the binding constants of the intracellular substrates decrease with increasing pH, at about the same rate as the extracellular substrates, supports the concept of a single, functional site for each substrate. For example, this relationship could be explained by a displacement of the binding site within the membrane, so that it becomes less accessible for the binding of substrates as the pH increases from 7.00 to 8.00. Furthermore, the concomitant increase in the electrical interaction constants α and β with the decrease in the binding affinity of these ions supports the idea of an access channel between the bulk and the binding sites for HCO_3^- and Na^+ that becomes narrower and more difficult to traverse as the pH increases. The electrical coefficients β and α represent the "electrical distance" between the membrane/water interface and the corresponding ion binding sites on the protein, expressed as a fraction of membrane thickness. Alternatively, they may represent the attenuation of the membrane's electric field at the ions' binding sites, due to the high dielectric aqueous environment in the access channel (Jordan, 1987). The increase in the electrical coefficients may thus reflect the decrease in hydration of the access channel as it becomes narrower at alkaline pH.

The increase in the value of the "effective charge" ($z\delta_z$) with increasing pH could potentially be explained by two mechanisms: 1) An increase in the net positive charge on the unloaded form of the carrier as the pH is increased. This possibility seems very unlikely, though, as one would expect a decrease rather than an increase in the net charge due to deprotonation of titratable amino acid groups on the carrier protein. 2) Considering that the "effective charge" on the unloaded form of the carrier moves in the membrane's electric field during the membrane translocation/reorientation step of the cotransporter, an increase in the interaction strength between the moving charge and the electric field would be manifested as an increase in the "effective charge." Such an increase in the interaction strength could result from a decrease in hydration state of the carrier as the pH is increased from 7.00 to 8.00.

Superficially, the biphasic profile of activation/inactivation of transport activity with pH (Fig. 3 *A*) is similar to the observed pH dependence of many hydrolytic enzymes. This analogy is of interest because pH-dependent activation/inactivation of enzymes is often well understood at the molecular level. For example, titration of amino acid residues involved in enzyme catalysis within the active site can be directly linked to rates of enzyme activity. Thus biphasic behavior with pH can come about by titration of one molecular group that activates and another one that inactivates (Chao and Graves, 1970; Ottolenghi, 1971). However, our attempts to fit the pH dependence of overall transport velocity (current), individual rate constants, or electrical parameters to a simple model involving titratable groups failed to give satisfactory results. This probably reflects an indirect and complex relationship between protonation of an amino acid and the rate of transport. After all, transport involves conformational changes of the transporter protein, and the rates of these conformational changes are likely to be only indirectly linked to the protonation state of specific amino acid residues.

We thank Dr. J. Whittembury, Bioanalytical Instrumentation, Cleveland, for the design of the Ussing chamber and Ms. Carol Bertrand for writing the computer program used to acquire the *I-V* relations.

This work was supported by a grant in aid from the American Heart Association and the Kidney Foundation of Ohio to EG and National Institutes of Health grants HL41618 and DK07678 to UH.

REFERENCES

Acevedo, M. 1994. Effect of acetyl choline on ion transport in sheep tracheal epithelium. *Pflugers Arch.* 427:543–546.

Alpern, R. J. 1985. Mechanism of basolateral membrane $H^+/OH^-/HCO_3^-$ transport in the rta proximal convoluted tubule. A sodium-coupled electrogenic process. *J. Gen. Physiol.* 86:613–636.

Alpern, R. J., and M. Chambers. 1986. Cell pH in the rat proximal convoluted tubule. Regulation by luminal and peritubular pH and sodium concentration. *J. Clin. Invest.* 78:502–510.

Aronson, P. S. 1983. Mechanisms of active H^+ secretion in the proximal tubule. *Am. J. Physiol.* 245:F647–F659.

Aronson, P. S., J. Nee, and M. A. Suhm. 1982. Modifier role of internal H^+ in activating the Na^+-H^+ exchanger in renal microvillus membrane vesicles. *Nature.* 299:161–163.

Backman, K., B. Harrison, M. Meysenberg, C. Schwartz, and W. Germann. 1992. Inactivation of a volume-sensitive basolateral potassium conductance in turtle colon: effect of metabolic inhibitors. *Biochim. Biophys. Acta.* 1105:89–96.

Bevington, P. R. 1969. Data Reduction and Error Analysis for the Physical Sciences. McGraw-Hill, New York. 314–315.

Biagi, B. A., and M. Sohtell. 1986. Electrophysiology of basolateral transport in the rabbit proximal tubule. *Am. J. Physiol.* 250:F267–F272.

Boorer, K. J., W. B. Frommer, D. R. Bush, M. Kreman, D. D. Loo, and E. M. Wright. 1996. Kinetics and specificity of a H^+/amino acid transporter from *Arabidopsis thaliana*. *J. Biol. Chem.* 271:2213–2220.

Boron, W. F., and E. L. Boulpaep. 1983a. Intracellular pH regulation in the renal proximal tubule of the salamander: basolateral HCO_3 transport. *J. Gen. Physiol.* 81:53–94.

Boron, W. F., and E. L. Boulpaep. 1983b. Intracellular pH regulation in the renal proximal tubule of the salamander. Na-H exchange. *J. Gen. Physiol.* 81:29–52.

Boron, W. F., and R. C. Knakal. 1989. Intracellular pH-regulating mechanism of the squid axon. Interaction between DNDS and extracellular Na and HCO_3. *J. Gen. Physiol.* 93:123–150.

Chao, J., and D. J. Graves. 1970. pH dependence of the kinetic parameters of maltodextrin phosphorylase. *Biochem. Biophys. Res. Commun.* 40: 1398–1403.

Coppola, S., and E. Frömter. 1994. An electrophysiological study of angiotensin II regulation of Na-HCO_3 cotransport and K conductance in renal proximal tubules. II. Effect of micromolar concentrations. *Pflugers Arch.* 427:151–156.

Emmett, M., R. J. Alpern, and D. W. Seldin. 1992. Metabolic acidosis. *In* The Kidney, Physiology and Pathophysiology. D. W. Seldin and G. Giebisch, editors. Raven Press Publishers, New York. 2759–2838.

Eskandari, S., D. D. Loo, G. Dai, O. Levy, E. M. Wright, and N. Carrasco. 1997. Thyroid Na^+/I^- symporter. Mechanism, stoichiometry, and specificity. *J. Biol. Chem.* 272:27230–27238.

Eyring, H., R. Lumry, and J. W. Woodbury. 1949. Some applications of modern rate theory to physiological systems. *Rec. Chem. Prog.* 10: 100–114.

Forster, I., N. Hernando, J. Biber, and H. Murer. 1998. The voltage dependence of a cloned mammalian renal type II Na^+/P_i cotransporter (NaP_i-2). *J. Gen. Physiol.* 112:1–18.

Grinstein, S., S. Cohen, and A. Rothstein. 1984. Cytoplasmic pH regulation in thymic lymphocytes by an amiloride-sensitive Na/H antiport. *J. Gen. Physiol.* 83:341–369.

Gross, E., and U. Hopfer. 1995. Regulation of Na rebasorption by Ang II: the role of the membrane potential. *J. Am. Soc. Nephrol.* 6:338A.

Gross, E., and U. Hopfer. 1996. Activity and stoichiometry of Na:HCO_3 cotransport in immortalized renal proximal tubule cells. *J. Membr. Biol.* 152:245–252.

Gross, E., and U. Hopfer. 1998. Voltage and co-substrate dependence of the Na-HCO_3 cotransportrer kinetics in renal proximal tubule cells. *Biophys. J.* 75:810–824.

Hager, K., A. Hazama, H. M. Kwon, D. D. Loo, J. S. Handler, and E. M. Wright. 1995. Kinetics and specificity of the renal Na^+/myo-inositol cotransporter expressed in *Xenopus* oocytes. *J. Membr. Biol.* 143: 103–113.

Illek, B., H. Fischer, and W. Clauss. 1993. Quinidine sensitive K+ channels in the basolateral membrane of embryonic coprodeum epithelium: regulation by aldosterone and thyroxine. *J. Comp. Physiol. B.* 163: 556–562.

Jordan, P. 1987. How pore mouth charge distributions alter the permeability of transmembrane ionic channels. *Biophys. J.* 51:297–311.

Kirk, K. L., and D. C. Dawson. 1983. Basolateral potassium channel in turtle colon: evidence for single file flow. *J. Gen. Physiol.* 82:297–313.

Klamo, E. M., M. E. Drew, S. M. Landfear, and M. P. Kavanaugh. 1996. Kinetics and stoichiometry of a proton/myo-inositol cotransporter. *J. Biol. Chem.* 271:14937–14943.

Läuger, P., and P. Jauch. 1986. Microscopic description of voltage effects on ion-driven cotransport systems. *J. Membr. Biol.* 91:275–284.

Mackenzie, B., D. D. Loo, Y. Fei, W. J. Liu, V. Ganapathy, F. H. Leibach, and E. M. Wright. 1996. Mechanisms of the human intestinal H^+-coupled oligopeptide transporter hPEPT1. *J. Biol. Chem.* 271: 5430–5437.

Mackenzie, B., D. D. Loo, and E. M. Wright. 1998. Relationships between Na^+/glucose cotransporter (SGLT1) currents and fluxes. *J. Membr. Biol.* 162:101–106.

Muller-Berger, S., M. Heyer, M. F. Romero, W. F. Boron, and E. Fromter. 1998. Stoichiometry of rat Na-HCO3 cotransporter (rkNBC) overexpressed in *Xenopus laevis* oocytes measured using giant patches. *J. Am. Soc. Nephrol.* 9:9A.

Ottolenghi, P. 1971. The effect of hydrogen ion concentration on the simplest steady-state enzyme systems. *Biochem. J.* 123:445–453.

Panayotova-Heiermann, M., D. D. Loo, and E. M. Wright. 1995. Kinetics of steady-state currents and charge movements associated with the rat Na^+/glucose cotransporter. *J. Biol. Chem.* 270:27099–27105.

Parent, L., S. Supplisson, D. D. F. Loo, and E. M. Wright. 1992. Electrogenic properties of the cloned Na^+/glucose cotransporter. II. A transport model under nonrapid equilibrium conditions. *J. Membr. Biol.* 125: 63–79.

Soleimani, M., G. A. Lesoine, J. A. Bergman, and T. D. McKinney. 1991. A pH modifier site regulates activity of the Na:HCO_3 cotransporter in basolateral membranes of kidney proximal tubule. *J. Clin. Invest.* 88: 1135–1140.

Woodbury, J. W. 1971. Eyring rate theory model of the current-voltage relationship of ion channels in excitable membranes. *In* Chemical Dynamics. J. O. Hirschfelder, editor. Wiley, New York. 601–617.

Woost, P. G., D. E. Orosz, W. Jin, P. S. Frisa, J. W. Jacobberger, J. G. Douglas, and U. Hopfer. 1996. Immortalization and characterization of proximal tubule cells derived from kidneys of spontaneously hypertensive and normotensive rats. *Kidney Int.* 50:125–134.

Yoshitomi, K., and E. Frömter. 1985. How big is the electrochemical potential difference of Na across rat renal proximal tubular cell membranes in vivo? *Pflugers Arch.* 405:S121–S126.

Yun, C. H. C., G. Lamprecht, D. V. Forster, and A. Sidor. 1998. NHE3 kinase A regulatory protein E3KARP binds the epithelial brush border Na^+/H^+ exchanger NHE3 and the cytoskeletal protein ezrin. *J. Biol. Chem.* 273:25856–25863.